J|A|C|S

Article

pubs.acs.org/JACS

Evolutionary Design of Low Molecular Weight Organic Anolyte Materials for Applications in Nonaqueous Redox Flow Batteries

Christo S. Sevov,[†,‡] Rachel E. M. Brooner,[†,‡,#] Etienne Chénard,[†,§,#] Rajeev S. Assary,[†,⊥] Jeffrey S. Moore,[†,§,∥] Joaquín Rodríguez-López,[†,§] and Melanie S. Sanford*,[†,‡]

[†]Joint Center for Energy Storage Research, Argonne, Illinois 60439, United States

[‡]Department of Chemistry, University of Michigan, 930 North University Avenue, Ann Arbor, Michigan 48109, United States

[§]Department of Chemistry, University of Illinois at Urbana-Champaign, Urbana, Illinois 61801, United States

[∥]Beckman Institute for Advanced Science and Technology, University of Illinois at Urbana-Champaign, Urbana, Illinois 61801, United States

[⊥]Materials Science Division, Argonne National Laboratory, Argonne, Illinois 60439, United States

Ⓢ Supporting Information

ABSTRACT: The integration of renewable energy sources into the electric grid requires low-cost energy storage systems that mediate the variable and intermittent flux of energy associated with most renewables. Nonaqueous redox-flow batteries have emerged as a promising technology for grid-scale energy storage applications. Because the cost of the system scales with mass, the electroactive materials must have a low equivalent weight (ideally 150 g/(mol·e^-) or less), and must function with low molecular weight supporting electrolytes such as $LiBF_4$. However, soluble anolyte materials that undergo reversible redox processes in the presence of Li-ion

supports are rare. We report the evolutionary design of a series of pyridine-based anolyte materials that exhibit up to two reversible redox couples at low potentials in the presence of Li-ion supporting electrolytes. A combination of cyclic voltammetry of anolyte candidates and independent synthesis of their corresponding charged-states was performed to rapidly screen for the most promising candidates. Results of this workflow provided evidence for possible decomposition pathways of first-generation materials and guided synthetic modifications to improve the stability of anolyte materials under the targeted conditions. This iterative process led to the identification of a promising anolyte material, N-methyl 4-acetylpyridinium tetrafluoroborate. This compound is soluble in nonaqueous solvents, is prepared in a single synthetic step, has a low equivalent weight of 111 g/(mol·e^-), and undergoes two reversible $1e^-$ reductions in the presence of $LiBF_4$ to form reduced products that are stable over days in solution.
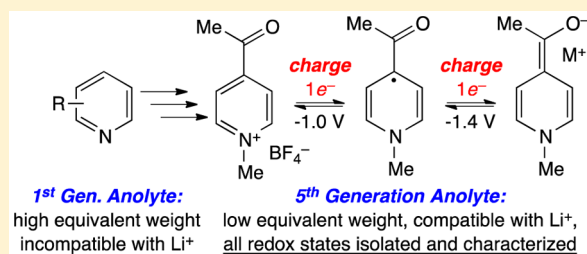
■ INTRODUCTION

Electrical energy is currently the single largest form of energy consumed worldwide,[1] and the consumption of electricity is predicted to double by 2050. These increasing global demands will require energy sources that do not contribute to the accumulation of greenhouse gases or to the exhaustion of the limited supply of fossil fuels.[2] To address this challenge, major effort is focused on the development of technologies that convert renewables into electrical energy.[3−6] However, the integration of renewables into the electrical grid remains limited due to the variable and intermittent nature of energy sources like solar and wind. Energy storage systems (ESSs) that respond rapidly to changes in flux from renewable sources will enable the large-scale penetration of renewables into the grid.

Redox-flow batteries (RFBs) represent a promising technology for grid-scale energy storage.[7−10] In RFBs, anolyte and catholyte fluids undergo electrochemical reactions as they are passed over a current collector. As a result, the capacity and power of the ESS scale independently, which reduces cost.

Increasing the volume of the electroactive solution increases the capacity of the system, while expanding the surface area of the current collector increases the power. These features mitigate mechanical fatigue, which is common in competing battery technologies that involve deposition and dissolution of electroactive materials at electrode surfaces. In addition, the physical separation of the electroactive materials in RFBs precludes exotherms that result from mixing.

These promising features of RFBs have motivated a techno-economic model that provides quantitative guidelines for cost-competitive grid-scale RFB storage systems.[11] According to the model, RFBs operating in nonaqueous media open up new design space by taking advantage of high cell potentials without decomposition of the solvent. To meet cost targets of $120/kW·h, supporting electrolytes with low molecular weight, such as $LiBF_4$ (MW = 94 g/mol), are preferred to $TBABF_4$ (TBA =

tetrabutylammonium, MW = 329 g/mol). Additionally, to meet cost and solubility targets, the anolyte and catholyte materials should have a molecular weight-to-charge ratio (also known as equivalent weight) that is less than 150 g per mole of stored charge g/(mol·e^-)). These techno-economic constraints motivate fundamental research to identify and understand the electrochemistry of small molecules that are highly soluble, are chemically compatible with Li-ion supports, and exhibit one or more reversible redox reactions at especially low (anolytes) or high (catholytes) potentials.
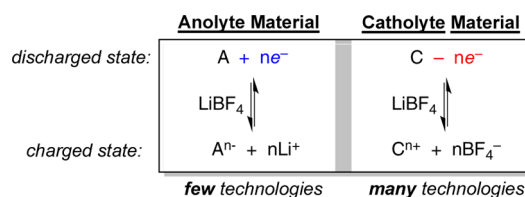

Figure 1. Representative half-cell reactions of RFB anolyte and catholyte materials in a lithium-ion supported media.

The use of organic molecules as soluble anolytes for RFBs is an attractive strategy for meeting the challenging molecular weight-to-charge goals. Persistent organic radicals have been known for more than a century,[12] and many soluble catholyte materials that exhibit reversible electrochemistry in Li-ion electrolytes are known (Figure 1).[13] Most catholyte systems employ molecules with extensive conjugation, such as quinones,[14−17] thioquinones,[18] arylamines,[19] alkoxyarenes,[20−22] thiophenes,[23−25] thiadiazoles,[26,27] and N-oxides.[28,29] The compatibility of these catholyte materials with Li-ion electrolytes and nonaqueous solvents has facilitated their coupling with other Li-ion half-cells (e.g., lithium intercalation supports and lithium metal).[7,30−32] In contrast, *anolyte* materials based on organic compounds that operate with Li-ion electrolytes are rare and currently remain limited to insoluble lithium salts of arylcarboxylates.[33−36]

In this report, we seek to address the underdevelopment of soluble organic anolyte materials that are compatible with Li-ion electrolytes. In addition, we target anolyte candidates that satisfy the cost constraints to equivalent weight. We address these challenges through an iterative workflow that employs the combination of cyclic voltammetry (to rapidly evaluate anolyte candidates) with chemical synthesis of charged anolyte materials (to monitor chemical stability and solubility). These studies have ultimately led to the identification of *N*-methyl 4-acetylpyridinium tetrafluoroborate: a molecule that exhibits two reversible redox couples in MeCN/LiBF$_4$. This compound is soluble in nonaqueous solvents at all charge states, is prepared from commercial materials in a single synthetic step, is stable over days at all charge states, and, at 111 g/(mol·e^-), falls significantly below the target equivalent weight of 150 g/(mol·e^-).

RESULTS AND DISCUSSION

Methods for Electrochemical Evaluation of Compounds. Our search for low molecular weight anolyte materials required the exploration of a significant range of chemical space. To do so in a rapid fashion, we initially screened a series of heteroarenes by cyclic voltammetry (CV). Electrochemical analysis was conducted in a three-electrode cell composed of a glassy carbon working electrode, a platinum

counter electrode, and a Ag/Ag$^+$ reference electrode. The CV of each anolyte candidate was initially conducted in acetonitrile (MeCN) with TBABF$_4$ as the supporting electrolyte. These results were then compared to those obtained in MeCN/LiBF$_4$ under otherwise identical conditions. The comparison of these electrochemical results provided a feedback loop that guided the iterative design of new generations of anolyte materials.

The chemical reversibility of each redox couple in the CV was estimated by calculating the ratio of the diffusion-limited peak-heights of the cathodic (i_{pc}) and anodic (i_{pa}) currents as a function of scan rate (Figure 2). Redox processes that generate
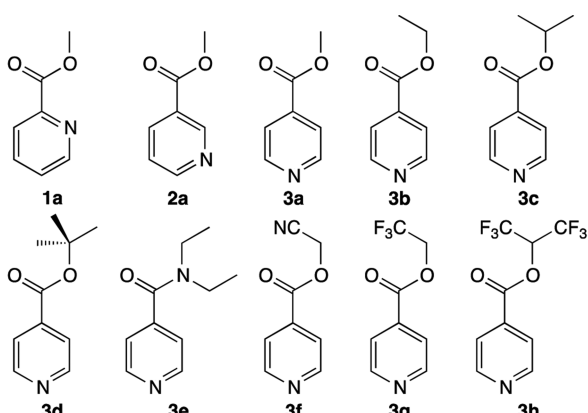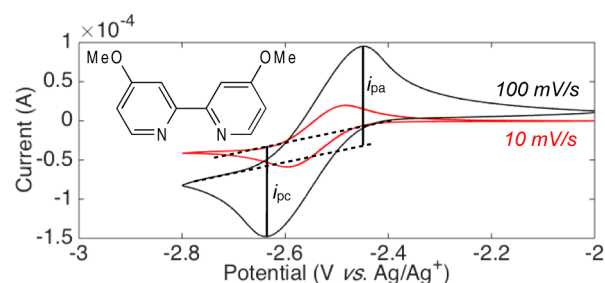

Figure 2. Reductive couple of 4,4′-methoxybipyridine (0.01 M) in MeCN with TBABF$_4$ (0.1 M) at 100 and 10 mV/s scan rates. Second cycles plotted: i_{pc}/i_{pc} at 100 mV = 1.02; i_{pc}/i_{pc} at 10 mV = 1.04.

reduced species with high persistence and stability generally exhibit current peak-height ratios close to one ($i_{pc}/i_{pa} \approx 1$). Chemical irreversibility is preliminarily identified by high i_{pc}/i_{pa} ratios that increase at slower scan rates. In addition to providing an initial estimate of reversibility, these metrics serve as a tool to rapidly screen and compare a series of prospective anolyte materials.

Evaluation of Pyridine Derivatives as Anolyte Materials. In the course of our studies of redox active metal-coordination complexes,[37,38] we discovered that a number of bipyridine derivatives exhibit reversible CVs. For example, the CV of 4,4′-dimethoxybipyridine displays a redox couple at low potential (−2.6 V versus Ag/Ag$^+$ in MeCN with TBABF$_4$ supporting electrolyte; Figure 2) with $i_{pc}/i_{pc} \approx 1$. On the basis of this preliminary result, we assessed the CVs of a series of lower molecular weight monopyridine analogues in MeCN/TBABF$_4$. No reduction was observed within the electrochemical window of MeCN for any pyridine derivative bearing an electron-donating group (EDG) at the 2- or 4-position (e.g., 4-methoxypyridine, 2-methoxypyridine, 4-methylpyridine, 2-methylpyridine; see Supporting Information for a full list of tested compounds). This led us to hypothesize that the electron-withdrawing pyridyl ring *ortho* to nitrogen in 4,4′-methoxybipyridine is critical for the observed redox couple. As such, we next explored pyridine derivatives bearing electron-withdrawing substituents. The redox potentials and current peak-height ratios at scan rates of 100 and 10 mV/s were determined for a series of picolinate (**1**), nicotinate (**2**), and isonicotinate (**3a−h**) derivatives and are summarized in Chart 1.

We first examined the effect of varying the position of an electron-withdrawing ester substituent in molecules **1a**, **2a**, and **3a** (Chart 1, entries 1−3). In MeCN/TBABF$_4$, all three compounds are reduced at standard potentials lower than −2 V vs Ag/Ag$^+$. No reoxidation current is observed for methyl nicotinate **2a**. The reduction of methyl picolinate **1a** shows partial chemical reversibility at 100 mV/s, but is completely

Chart 1. Ratios of Current Peak Heights from CV for Alkyl Pyridinecarboxylates

entry	compound[a]	solvent/support[b]	E_1^0 (V)[c]	i_{pc1}/i_{pa1}[d] (100 mV/s)	i_{pc1}/i_{pa1}[d] (10 mV/s)
1	**1a**	MeCN/TBABF$_4$	-2.36	1.83	>5
2	**2a**	MeCN/TBABF$_4$	---[e]	>5	>5
3	**3a**	MeCN/TBABF$_4$	-2.16	1.15	1.67
4	**3b**	MeCN/TBABF$_4$	-2.20	1.03	1.28
5	**3c**	MeCN/TBABF$_4$	-2.20	1.02	1.10
6	**3d**	MeCN/TBABF$_4$	-2.24	1.01	1.09
7	**3e**	MeCN/TBABF$_4$	-2.52	1.18	>5
8	**3f**	MeCN/TBABF$_4$	---[e]	>5	>5
9	**3g**	MeCN/TBABF$_4$	-2.03	1.91	>5
10	**3h**	MeCN/TBABF$_4$	---[e]	>5	>5
11	**3a**	PC/TBABF$_4$	-2.40	1.35	2.02
12	**3a**	MeCN/LiBF$_4$	---[e]	>5	>5
13	**3a**	PC/LiBF$_4$	---[e]	>5	>5

[a]0.01 M substrate. [b]0.10 M TBABF$_4$ or LiBF$_4$ support. [c]E_1^0 is calculated as $(E_{1c} + E_{1a})/2$ and referenced to Ag/Ag$^+$. [d]Ratios were calculated for the second cycle following deconvolution of the voltammogram. [e]No anodic current was observed.

irreversible at the lower 10 mV/s scan rate. Methyl isonicotinate **3a**, exhibits a redox couple with significantly improved reversibility over **1a** and **2a**, even at scan rates of 10 mV/s (Chart 1, entry 3).

We next explored the impact of the ester substituent on the electrochemical behavior of isonicotinates **3a**−**h**. The methyl, ethyl, isopropyl, and *tert*-butyl esters all show reductions at comparable potentials (approximately −2.2 V; Figure 3). A sequential improvement in current peak-height ratio is observed upon moving from the methyl (**3a**) to ethyl (**3b**)
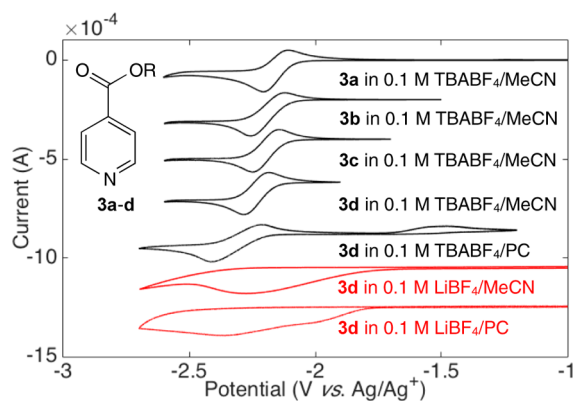

Figure 3. Voltammograms of selected isonicotinates. Conditions: second cycles plotted for CVs of 0.01 M **3a**−**d** in specified media at 10 mV/s scan rate.

to isopropyl (**3c**) to *tert*-butyl (**3d**) derivative (Chart 1, entries 3−6 and Figure 3). In contrast, reductions of esters bearing the electron-withdrawing cyanoethyl, trifluoroethyl, and hexafluoroisopropyl substituents appear at approximately −2.0 V and are all irreversible (entries 8−10). Replacement of the ester with a less electron-withdrawing diethylamide substituent (**3e**) results in a significant lowering of the reduction potential (to −2.5 V); however, this redox couple is irreversible at lower scan rates (entry 7).

The electrochemical data for **3a**−**h** provides insight into possible mechanisms for decomposition of the radical anion that is formed following reduction. Decomposition could occur by either homolytic or heterolytic cleavage of bonds in the ester moiety (Figure 4).[39,40] Homolytic cleavage of the O−R bond
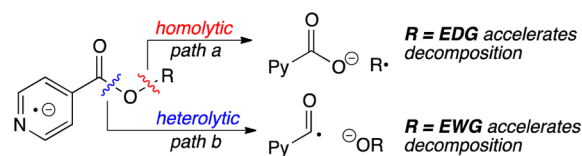

Figure 4. Two possible decomposition pathways for the reduced anolytes (isonicotinate radical anions). The experimental data is more consistent with pathway b.

(Figure 4, top) would generate a carboxylate and an alkyl radical. According to this proposition, accelerated decomposition is expected for compounds with EDGs (which stabilize the alkyl radical) and retarded by EWGs. Conversely, heterolytic cleavage of the (O)C−O bond releases an alkoxide anion (Figure 4, bottom). Accelerated decomposition by this pathway is expected for compounds with EWGs that stabilize the alkoxide. Our experimental results show that isonicotinates bearing electron withdrawing ester substituents (**3f**−**h**) exhibit irreversible electrochemistry (Chart 1, entries 8−10). Furthermore, the electrochemical behavior of the *tert*-butyl analogue **3d** is superior to that of the methyl analogue **3a** (Chart 1, entries 6 vs 3). These data are most consistent with decomposition pathway b in Figure 4.

Evaluation of N-Protected Isonicotinates as Anolyte Materials with LiBF$_4$ Electrolyte. Compound **3d** displays the most promising electrochemistry of the tested compounds in MeCN/TBABF$_4$. Thus, we next performed CV of this compound in MeCN/LiBF$_4$ and propylene carbonate (PC)/LiBF$_4$ (Figure 3). Although the cathodic wave in Figure 3 suggests that reduction generates a similar radical anion to that in TBABF$_4$, no corresponding anodic wave is observed for CVs in solutions with LiBF$_4$.

A recent report has shown that the complexation of BF$_3$ to the nitrogen of quinoxaline dramatically increases the reversibility of its reduction in Li-ion electrolytes.[41] On the basis of this report, we hypothesized that analogous behavior might be observed for the isonicotinate series. To test this possibility, the isonicotiate−BF$_3$ adducts **4a**−**d** were synthesized and analyzed by CV, and the results are summarized in entries 1−6 of Chart 2. The methyl and *tert*-butyl analogues **4a** and **4d** were initially examined in MeCN/TBABF$_4$. In this media, the first reductive couple appears at approximately −1.8 V, with current peak-height ratios approaching unity for both materials. In MeCN/LiBF$_4$, the couple shifts to approximately −1.4 V, but the current ratios remain close to 1, even at the slow 10 mV/s scan rate (Chart 2, entries 3−6).

Chart 2. Current Peak Height Ratios from CV for BF₃-Adducts and N-Oxides of Isonicotinates

R = ⅗-BF₃: **4a**   **4b**   **4c**   **4d**
R = ⅗-O⁻ : **5a**   **5b**   **5c**   **5d**

entry	compound[a]	solvent/support[b]	E_1^0 (V)[c]	i_{pc1}/i_{pa1}[d] (100 mV/s)	i_{pc1}/i_{pa1}[d] (10 mV/s)
1	4a	MeCN/TBABF₄	-1.62	1.03	1.10
2	4d	MeCN/TBABF₄	-1.65	1.03	1.05
3	4a	MeCN/LiBF₄	-1.43	1.02	1.06
4	4b	MeCN/LiBF₄	-1.40	1.06	1.08
5	4c	MeCN/LiBF₄	-1.40	1.06	1.09
6	4d	MeCN/LiBF₄	-1.44	1.06	1.11
7	5a	MeCN/TBABF₄	-1.96	1.05	1.41
8	5d	MeCN/TBABF₄	-2.01	1.00	1.17
9	5a-5d	MeCN/LiBF₄	---[e]	>5	>5

[a] 0.01 M substrate. [b] 0.10 M TBABF₄ or LiBF₄ support. [c] E_1^0 is calculated as $(E_{1c} + E_{1a})/2$ and referenced to Ag/Ag⁺. [d] Ratios were calculated for the second cycle following deconvolution of the voltammogram. [e] No anodic current was measured.

One disadvantage of the BF₃ adducts is their high molecular weight. For instance, the equivalent weight of **4d** as a single electron anolyte is 247 g/(mol·e⁻), which significantly exceeds the target of 150 g/(mol·e⁻). In an attempt to address this issue, we scanned to more negative potentials to explore the possibility of charging **4d** with a second electron. While a second reduction is observed at −2.3 V, reoxidation occurs with a much lower i_{pa} (red trace in Figure 5). Nonetheless, these data demonstrate that N-functionalized isonicotinates exhibit multiple redox processes at low potentials in MeCN/LiBF₄.
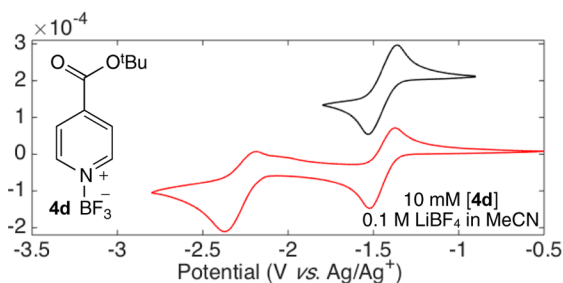

Figure 5. (a) CVs of **4d** through one (black trace) and two (red trace) redox couples with LiBF₄ supporting electrolyte. Conditions: 100 mV/s scan rate.

We next examined the substitution of BF₃ with lower molecular weight substituents on nitrogen, starting with N-oxide derivatives. In MeCN/TBABF₄, the alkyl isonicotinate-N-oxides **5a–d** undergo a single reduction at approximately −2 V, with current peak-height ratios close to one (Chart 2, entries 7–8).[42] However, this reduction is irreversible in MeCN/LiBF₄ (Chart 2, entry 9).

We noted that the weak N−O bond[43] of the N-oxide is susceptible to many side reactions. As a result, we next targeted N-alkylpyridinium salts. These molecules offer the advantage

that the N-alkyl bond is much stronger than that of N-oxides or BF₃-adducts. In addition, literature reports have shown that a variety of pyridinium salts undergo one-electron chemical reduction to form stable radical intermediates.[44,45] Furthermore, a CV study of related pyridinium salts in MeCN with tetrabutylammonium salts demonstrated the accessibility of a second, reversible reduction.[46]

N-Ethylpyridinium iodide salts **6a,b** were synthesized by reactions of **3a–d** with iodoethane. CV of these materials in MeCN/LiBF₄ revealed a reversible redox couple at −1.1 V with peak height ratios close to one (Chart 3, entries 1 and 2). Upon

Chart 3. Current Peak Height Ratios for Isonicotinates As Determined by Cyclic Voltammetry

X = I : **6a**   **6b**   --   --   --
X = PF₆: **7a**   **7b**   **7c**   **7d**   --
X = BF₄: **8a**   --   --   --   **9a**

entry	compound[a]	solvent/support[b]	E_1^0 (V)[c]	i_{pc1}/i_{pa1}[e] (10 mV/s)	E_2^0 (V)[d]	i_{pc2}/i_{pa2}[e] (10 mV/s)
1	6a	MeCN/LiBF₄	-1.11	0.99	-1.85	0.95
2	6b	MeCN/LiBF₄	-1.10	0.98	-1.86	0.94
3	7a	MeCN/LiBF₄	-1.11	0.98	-1.88	0.96
4	7b	MeCN/LiBF₄	-1.11	0.99	-1.90	0.96
5	7c	MeCN/LiBF₄	-1.13	0.97	-1.89	0.95
6	7d	MeCN/LiBF₄	-1.15	0.99	-1.93	0.93
7	8a	MeCN/LiBF₄	-1.11	0.98	-1.89	0.95
8	9a	MeCN/LiBF₄	-1.10	0.99	-1.83	0.98

[a] 0.01 M substrate. [b] 0.10 M LiBF₄ support. [c] E_1^0 is calculated as $(E_{1c} + E_{1a})/2$. [d] E_2^0 is calculated as $(E_{2c} + E_{2a})/2$ and referenced to Ag/Ag⁺. [e] Ratios were calculated for the second cycle following deconvolution of the voltammogram.

scanning to more negative potentials, a second couple was observed at −1.9 V. In contrast to the BF₃−adducts, compounds **6a−d** exhibit well-shaped anodic peaks after this second reduction with $i_{pc}/i_{pa} \approx 0.95$ at scan rates of 10 mV/s.

The voltammograms of the iodide salts also show an additional current response at lower potentials. Undesirable redox processes of the iodide counterion were suspected. To test this hypothesis, we next prepared the hexafluorophosphate (PF₆) analogues **7a−d** by salt metathesis of the iodide salts with NH₄PF₆ to exchange the iodide counterion. Voltammograms of these compounds exhibit more ideal behavior compared to those of the iodide analogues, and the identity of the counterion does not appear to influence the peak height ratios for the N-ethylpyridinium (Chart 3, entries 3−6). In addition, unlike with compounds **3a−d**, substitution of the carboxylate or at nitrogen has minimal influence on the current peak height ratios for the two redox couples (Chart 3, entries 3−6, 10 mV/s). As a result, N-methyl isonicotinate **9a** with a BF₄ counterion was prepared. This molecule has the lowest equivalent weight (127 g/(mol·e⁻)) of the isonicotinate salts studied while maintaining analogous electrochemical properties to those of **6a**, **7a**, and **8a** (Chart 3, entry 8).[47]

Synthesis, Solubility, and Stability of Anolyte 9a and Its Reduced Analogue 9a⁽⁻⁾. The isonicotinate salt **9a** was prepared in a single step from the reaction of methyl

isonicotinate with trimethyloxonium tetrafluoroborate in dichloromethane. This air- and moisture-stable solid precipitates over the course of the reaction, and is isolated on a gram scale via simple filtration.

The CV of **9a** was measured in both MeCN/LiBF$_4$ and PC/LiBF$_4$ (Figure 6, *i* and *ii*, respectively). Although two reductive
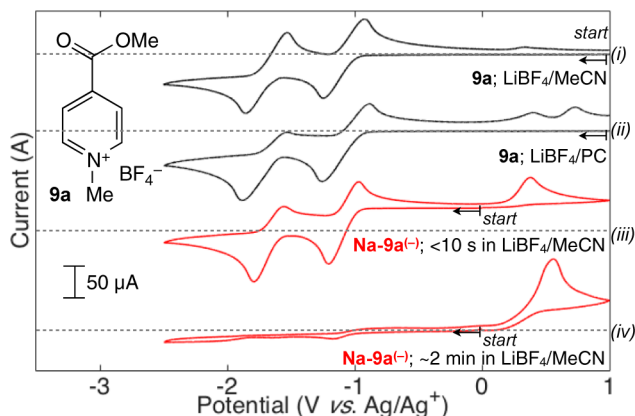

Figure 6. CVs of **9a** in MeCN (*i*) or PC (*ii*). CV of **9a**$^{(-)}$ immediately after dissolution in MeCN (*iii*) and 2 min later (*iv*). Conditions: 0.01 M **9a** or **Na-9a**$^{(-)}$ with 0.1 M LiBF$_4$ in the specified solvent at 100 mV/s scan rate. First cycles are plotted. Gray dashed lines indicate the axis of origin. Arrows indicate start and direction of CV scan.

waves are observed in both solvents, the chemical reversibility of the second reduction is lower in PC than in MeCN. Furthermore, the CV in PC shows the presence of byproducts that undergo oxidation at positive potentials (Figure 6, *ii*). These initial results warranted further studies of the solubility and stability of **9a** in MeCN.

As discussed above, the CV experiments were used as an initial screen for the accessibility and reversibility of reductive couples for anolyte candidates. However, for a redox flow battery application, it is crucial to have more detailed information about the long-term stability of the reduced species. As such, our next efforts focused on chemically generating **9a**$^{(-)}$, the material formed upon the $2e^-$ reduction of **9a**. The addition of sodium metal to a white suspension of **9a** in THF resulted in the formation of a red solution within 30 min at room temperature. After filtration, the red solution was concentrated to yield a dark orange solid. Analysis by ^{1}H NMR spectroscopy and elemental analysis confirmed the formation of the diamagnetic sodium salt **Na-9a**$^{(-)}$ (Scheme 1).

The CV of a freshly prepared solution of **Na-9a**$^{(-)}$ in MeCN/LiBF$_4$ shows peaks at −1.1 and −1.8 V, analogous to those observed for **9a** (Figure 6, *iii*). However, when the red solution of **Na-9a**$^{(-)}$ in MeCN/LiBF$_4$ is allowed to stand for 2 min, it changes color from red to brown, suggesting that decomposition is occurring. Consistent with this hypothesis,

Scheme 1. Chemical Reduction of 9a, and Decomposition Pathways of 9a$^{(-)}$
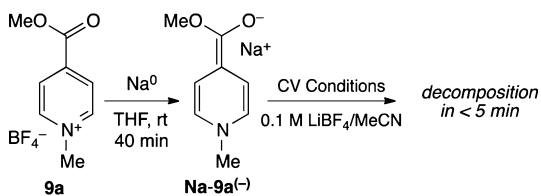
the CV of this brown solution shows no redox couples characteristic of **9a**. Instead, a single, irreversible oxidation at +0.5 V is observed (Figure 6, *iv*). These data demonstrate that the charged anolyte **Na-9a**$^{(-)}$ is unstable in MeCN/LiBF$_4$.

We next conducted studies to gain insight into the decomposition pathways of **Na-9a**$^{(-)}$ in MeCN/LiBF$_4$. Preliminary analysis of the material responsible for the anodic current at +0.5 V was performed using ^{1}H NMR spectroscopy and CV. While multiple decomposition products are observed by ^{1}H NMR spectroscopy, ^{1}H−^{1}H NMR COSY experiments show resonances that are consistent with products of protonation alpha to the carbonyl. The decomposition of **Na-9a**$^{(-)}$ via protonation was further explored by conducting CV with water intentionally added to the electrolyte solution. These studies revealed that CVs of **Na-9a**$^{(-)}$ in MeCN/LiBF$_4$ with 22 mM of added water are identical to those shown in Figure 6, *iv*. Notably, this decomposition process persists even upon our most rigorous attempts to dry the electrolyte solution.[48] These data suggest that the basicity of **Na-9a**$^{(-)}$ (which is an ester enolate) is sufficiently high to react with trace amounts of water and/or the MeCN solvent (pK_a^{49} ∼ 31).[50]

Synthesis, Solubility, and Stability of Anolyte 10a and Its Reduced Analogues 10a$^{(•)}$ and 10a$^{(-)}$. To minimize this proposed decomposition pathway, we next targeted anolyte materials that are less basic in their fully reduced form. It is well know that ketone enolates are approximately 3 orders of magnitude less basic than the analogous ester enolates. For example, the pK_a's of acetone and ethyl acetate are 26.5 and 29.5, respectively.[51] As such, we hypothesized that the reduced species derived from ketone analogues of **9a** would exhibit increased stability under the electrochemical conditions.

To test this hypothesis, the acetylpyridinium salt **10a** was prepared in 93% yield via methylation of 4-acetylpyridine with trimethyloxonium tetrafluoroborate. The CV of **10a** in MeCN/LiBF$_4$ shows two reductive couples with peak height ratios close to 1 (Figure 7, *i*). A direct comparison of **9a** and **10a**
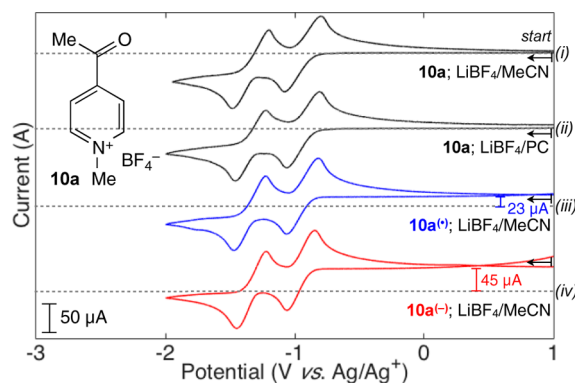

Figure 7. CVs of **10a** in MeCN (*i*) and PC (*ii*). CVs of **10a**$^{(•)}$ (*iii*) and **10a**$^{(-)}$ (*iv*) in MeCN. Conditions: 0.01 M **10a**, **10a**$^{(•)}$, or **10a**$^{(-)}$ with 0.1 M LiBF$_4$ in the specified solvent at 100 mV/s scan rate. First cycles are plotted. Gray dashed lines indicate the axis of origin. Arrows indicate start and direction of CV scan.

reveals that the first reductions occur at similar potentials (0.1 V difference) but that the second reduction of **10a** is 0.4 V more positive than that of **9a**. Notably, the CV of **10a** in PC/LiBF$_4$ shows reversible couples at comparable potentials to those in MeCN/LiBF$_4$ (Figure 7, *ii*). In contrast, as discussed above, the CV of **9a** in PC/LiBF$_4$ is indicative of significant decomposition (Figure 6, *ii*).

We next independently synthesized the materials generated during the reduction of **10a**. Compound **Na-10a**$^{(-)}$ was prepared via the $2e^-$ reduction of **10a** with sodium metal in THF. The product was isolated in 88% yield as an orange solid, and was characterized by elemental analysis, NMR spectroscopy, UV−vis spectroscopy, and CV. The ^{1}H NMR resonances of **Na-10a**$^{(-)}$ are shifted upfield relative to those of **10a**, consistent with a disruption of aromaticity (Figure 8, panel c vs b).
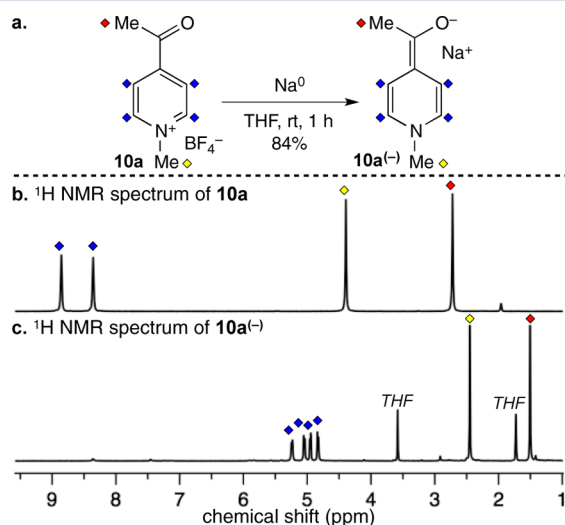

Figure 8. (a) Synthesis of **Na-10a**$^{(-)}$ by chemical reduction of **10a**. (b) ^{1}H NMR spectrum of **10a** and labeled resonances. (c) ^{1}H NMR spectrum of **Na-10a**$^{(-)}$ and labeled resonances.

Furthermore, all four protons on the ring of **Na-10a**$^{(-)}$ are inequivalent. This is consistent with an enolate structure, in which the carbonyl is not freely rotating. The CV of **Na-10a**$^{(-)}$ in MeCN/LiBF$_4$ shows two couples at identical potentials to **10a** (Figure 7, *iv*). In addition, CVs measured at starting potentials of +1 V show baseline currents of 40−50 μA. This non-zero initial current is consistent with the presence of a prereduced material (**Na-10a**$^{(-)}$) that undergoes oxidation at high potentials. Importantly, no analogous current is observed at +1 V when the material is in its discharged state **10a** (compare baseline currents relative to 0 μA lines in Figure 7, *i* vs *iv*). Unlike with **Na-9a**$^{(-)}$, the CV of **Na-10a**$^{(-)}$ does not change after standing in MeCN/LiBF$_4$ for 20 min at room temperature. This indicates that **Na-10a**$^{(-)}$ is stable under these conditions.

We also sought to prepare **10a**$^{(•)}$, which is the intermediate redox-state between the fully charged and discharged states of **10a**. In the literature, related *N*-alkylpyridine radicals have been generated electrochemically[52] or via chemical reduction with magnesium or zinc.[53,54] However, these methods generally afford the radical products in low yields. As such, we pursued an alternative strategy to prepare **10a**$^{(•)}$, involving comproportionation of **10a** and **Na-10a**$^{(-)}$ (Figure 9a). The dissolution of equimolar quantities of **10a** (a white solid) and **Na-10a**$^{(-)}$ (an orange solid) in MeCN resulted in the instantaneous formation of a dark green solution. Dilution of this solution with diethyl ether led to the precipitation of NaBF$_4$. The solution was then collected, and the solvent was removed to afford **10a**$^{(•)}$ as a dark green solid in 91% yield.

The neutral radical **10a**$^{(•)}$ was characterized by elemental analysis, ^{1}H NMR spectroscopy, EPR spectroscopy, UV−vis spectroscopy, and CV. As expected for a free radical, no
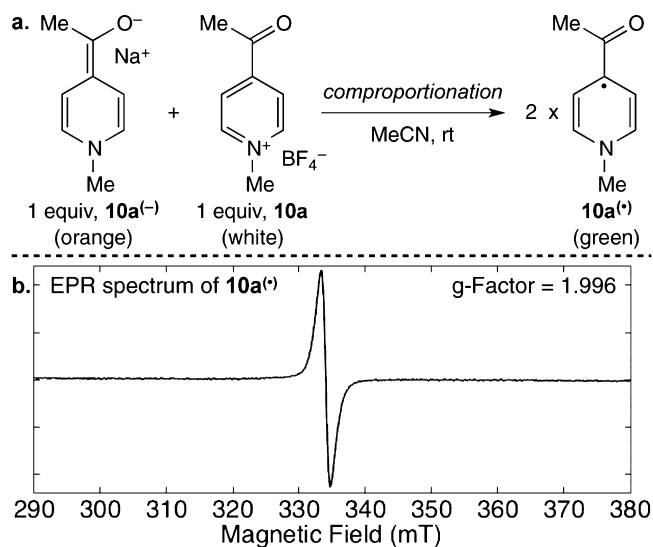

Figure 9. (a) Synthesis of **10a**$^{(•)}$ by comproportionation of **10a** and **Na-10a**$^{(-)}$. (b) EPR spectrum of a 1.0 mM solution of **10a**$^{(•)}$ in MeCN at 130 K.

resonances are observed in the ^{1}H NMR spectrum of **10a**$^{(•)}$. The EPR spectrum of a frozen solution of **10a**$^{(•)}$ in MeCN shows a strong isotropic resonance (Figure 9b). This signal is centered at 334 mT, and corresponds to a *g*-factor of 1.996. This value is consistent with a carbon centered radical, which generally has a *g*-factor near the value of a free electron (2.0036).[55]

A comparison of the CV of **10a**$^{(•)}$ to that of **10a** and **Na-10a**$^{(-)}$ shows two couples at identical potentials (Figure 7, *iii*).[56] Similar to **Na-10a**$^{(-)}$, a non-zero current is observed at the initial scanning potential of +1 V. This current (23 μA) is half of the initial current (45 μA) measured for **Na-10a**$^{(-)}$ at the same potential (compare baselines of CVs in Figure 7 *iii* vs *iv*). At the initial potential of +1 V, the reduced species **Na-10a**$^{(-)}$ undergoes two, $1e^-$ oxidations, while **10a**$^{(•)}$ undergoes only one, $1e^-$ oxidation. As such, these data are consistent with the different redox states of the molecule.

With **10a**, **10a**$^{(•)}$, and **Na-10a**$^{(-)}$ in hand, we next quantitatively assessed solubility and stability at each oxidation state. The solubilities of **10a**, **10a**$^{(•)}$, and **Na-10a**$^{(-)}$ were determined by UV−vis spectroscopy in MeCN under an inert atmosphere. A solubility of 1.6 ± 0.1 M in MeCN was measured for the parent compound **10a** by analyzing the UV absorbance at 281 nm.[57] This corresponds to 0.94 kg of a one-electron anolyte material per 1 kg of solvent, which exceeds the target of 0.8 kg anolyte per 1 kg solvent required to meet an RFB system price target of $120/kW·h.[11] In addition to these solubility parameters, the low equivalent weight of 111 g/(mol·e^-) for **10a** is well below the target limit of 150 g/(mol·e^-).

A saturated solution of **10a**$^{(•)}$ was prepared and analyzed at 322 nm by UV−vis spectroscopy. The saturation concentration of **10a**$^{(•)}$ was 5.4 ± 0.5 M. An analogous study with **Na-10a**$^{(-)}$ (monitoring the absorbance at 426 nm) revealed a solubility of 62 ± 7 mM. We believe that the low solubility of **Na-10a**$^{(-)}$ is partially a reflection of the Na$^+$ counterion, which is not the charge-balancing counterion during electrochemical reduction in solutions with a LiBF$_4$ support. Consistent with this proposal, a moderate increase in the solubility of **Na-10a**$^{(-)}$ (to 80 ± 6 mM) was observed using a 0.1 M solution of LiBF$_4$ in MeCN as the solvent. Nonetheless, the solubility of the

doubly reduced anolyte will clearly need to be enhanced prior to battery cycling studies at high concentration. Both literature precedent[21,37,58,59] and our preliminary results suggest that this will be feasible by appending solubilizing substituents on the scaffold of **10a**.[60]

The stabilities of **10a**, **10a**[(•)], and **Na-10a**[(−)] as solutions in MeCN were investigated by ^{1}H NMR spectroscopy or UV−vis spectroscopy. Separate solutions of **10a**, **10a**[(•)], and **Na-10a**[(−)] in MeCN were prepared at 480, 540, and 39 mM concentrations, respectively. The parent compound **10a** was monitored by ^{1}H NMR spectroscopy against an internal standard of 1,3,5-trimethoxybenzene. No measurable decomposition was detected over 4 days even in the presence of air and moisture. Solutions of the reduced species **10a**[(•)] and **Na-10a**[(−)] were stored at room temperature under nitrogen, and the concentrations of the solutions were measured periodically over 36 or 48 h by UV−vis spectroscopy (Figure 10). During
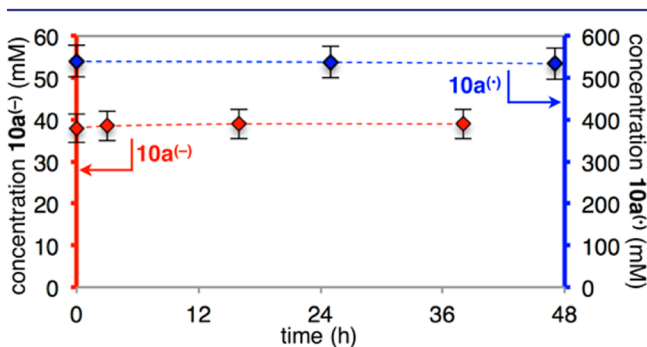

Figure 10. Concentrations of **10a**[(•)] (540 mM initial concentration, blue) and **Na-10a**[(−)] (39 mM initial concentration, red) in MeCN measured by UV−vis over 36−48 h.

this period, the concentrations of the reduced anolytes did not change, indicating that these materials are also stable and amenable to storage for days in solution. Furthermore, CVs of solutions of **10a**[(•)] and **Na-10a**[(−)] that were stored for 2 months in MeCN exhibited identical traces to those of the freshly prepared solutions. Importantly, these materials are also stable in mixed redox states. For example, CVs of mixtures of **10a** and **10a**[(•)] as well as of **10a**[(•)] and **Na-10a**[(−)] showed no detectable impurities after aging at room temperature for 16 h in MeCN/LiBF$_4$.

CONCLUSIONS

In conclusion, this report describes an iterative workflow that enabled the design of anolyte materials with tailored electrochemical properties. Specifically, we report an all-organic anolyte that undergoes two reversible reductions in solutions with Li-ion electrolytes. An initial systematic evaluation of anolyte candidates by CV led us from materials based on free pyridines to BF$_3$−pyridine adducts, pyridine *N*-oxides, *N*-ethyl isonicotinate salts of iodide, PF$_6$, and BF$_4$, and ultimately *N*-methyl acetylpyridinium BF$_4$ salts. These latter materials address the challenge of identifying soluble anolytes that operate in Li-ion supports and that have equivalent weights below 150 g/(mol·e^-).[11]

Over the course of these studies, we developed synthetic procedures to access the materials in their singly and doubly reduced states. Studies on these materials allowed us to identify decomposition pathways of isonicotinate salts. These decomposition pathways were resolved by preparing acetylpyridinium

salts. The latter materials are stable in their singly and doubly reduced states for days without measurable decomposition. Advanced electrochemical analysis and implementation of these materials in battery devices is currently ongoing and will be reported in due course.

ASSOCIATED CONTENT

Ⓢ Supporting Information

The Supporting Information is available free of charge on the ACS Publications website at DOI: 10.1021/jacs.5b09572.

> Experimental procedures and characterization of all new compounds including spectroscopic data and potentiometric data (PDF)

AUTHOR INFORMATION

Corresponding Author
*mssanfor@umich.edu

Author Contributions
#R.E.M.B. and E.C. contributed equally.

Notes
The authors declare no competing financial interest.

ACKNOWLEDGMENTS

REFERENCES

(1) Yang, Z.; Zhang, J.; Kintner-Meyer, M. C. W.; Lu, X.; Choi, D.; Lemmon, J. P.; Liu, J. *Chem. Rev.* **2011**, *111*, 3577.
(2) Dunn, B.; Kamath, H.; Tarascon, J.-M. *Science* **2011**, *334*, 928.
(3) Lin, Y.; Li, Y.; Zhan, X. *Chem. Soc. Rev.* **2012**, *41*, 4245.
(4) Huang, X.; Qi, X.; Boey, F.; Zhang, H. *Chem. Soc. Rev.* **2012**, *41*, 666.
(5) Li, G.; Zhu, R.; Yang, Y. *Nat. Photonics* **2012**, *6*, 153.
(6) Cappillino, P. J.; Pratt, H. D.; Hudak, N. S.; Tomson, N. C.; Anderson, T. M.; Anstey, M. R. *Adv. Energy Mater.* **2014**, *4*, 1300566.
(7) Wei, X. L.; Cosimbescu, L.; Xu, W.; Hu, J. Z.; Vijayakumar, M.; Feng, J.; Hu, M. Y.; Deng, X. C.; Xiao, J.; Liu, J.; Sprenkle, V.; Wang, W. *Adv. Energy Mater.* **2015**, *5*, 1400678.
(8) Ponce de León, C.; Frías-Ferrer, A.; González-García, J.; Szánto, D. A.; Walsh, F. C. *J. Power Sources* **2006**, *160*, 716.
(9) Shin, S.-H.; Yun, S.-H.; Moon, S.-H. *RSC Adv.* **2013**, *3*, 9095.
(10) Wang, W.; Luo, Q.; Li, B.; Wei, X.; Li, L.; Yang, Z. *Adv. Funct. Mater.* **2013**, *23*, 970.
(11) Darling, R. M.; Gallagher, K. G.; Kowalski, J. A.; Ha, S.; Brushett, F. R. *Energy Environ. Sci.* **2014**, *7*, 3459.
(12) Gomberg, M. *Chem. Rev.* **1924**, *1*, 91.
(13) Song, Z.; Zhou, H. *Energy Environ. Sci.* **2013**, *6*, 2280.
(14) Huskinson, B.; Marshak, M. P.; Suh, C.; Er, S.; Gerhardt, M. R.; Galvin, C. J.; Chen, X.; Aspuru-Guzik, A.; Gordon, R. G.; Aziz, M. J. *Nature* **2014**, *505*, 195.
(15) Wain, A. J.; Wildgoose, G. G.; Heald, C. G. R.; Jiang, L.; Jones, T. G. J.; Compton, R. G. *J. Phys. Chem. B* **2005**, *109*, 3971.
(16) Li, Q.; Batchelor-McAuley, C.; Lawrence, N. S.; Hartshorne, R. S.; Compton, R. G. *Chem. Commun.* **2011**, *47*, 11426.
(17) Fujinaga, T.; Izutsu, K.; Nomura, T. *J. Electroanal. Chem. Interfacial Electrochem.* **1971**, *29*, 203.
(18) Iordache, A.; Maurel, V.; Mouesca, J.-M.; Pécaut, J.; Dubois, L.; Gutel, T. *J. Power Sources* **2014**, *267*, 553.
(19) Feng, J. K.; Cao, Y. L.; Ai, X. P.; Yang, H. X. *J. Power Sources* **2008**, *177*, 199.
(20) Nesvadba, P.; Folger, L. B.; Maire, P.; Novák, P. *Synth. Met.* **2011**, *161*, 259.

(21) Huang, J.; Cheng, L.; Assary, R. S.; Wang, P.; Xue, Z.; Burrell, A. K.; Curtiss, L. A.; Zhang, L. *Adv. Energy Mater.* **2015**, *5*, 1401782.

(22) Huang, J. H.; Shkrob, I. A.; Wang, P. Q.; Cheng, L.; Pan, B. F.; He, M. N.; Liao, C.; Zhang, Z. C.; Curtiss, L. A.; Zhang, L. *J. Mater. Chem. A* **2015**, *3*, 7332.

(23) Henderson, J. C.; Kiya, Y.; Hutchison, G. R.; Abruña, H. D. *J. Phys. Chem. C* **2008**, *112*, 3989.

(24) Burkhardt, S. E.; Conte, S.; Rodriguez-Calero, G. G.; Lowe, M. A.; Qian, H.; Zhou, W.; Gao, J.; Hennig, R. G.; Abruna, H. D. *J. Mater. Chem.* **2011**, *21*, 9553.

(25) Hernández-Burgos, K.; Rodríguez-Calero, G. G.; Zhou, W.; Burkhardt, S. E.; Abruña, H. D. *J. Am. Chem. Soc.* **2013**, *135*, 14532.

(26) Gao, J.; Lowe, M. A.; Conte, S.; Burkhardt, S. E.; Abruña, H. D. *Chem. - Eur. J.* **2012**, *18*, 8521.

(27) Kiya, Y.; Henderson, J. C.; Abruña, H. D. *J. Electrochem. Soc.* **2007**, *154*, A844.

(28) Nakahara, K.; Oyaizu, K.; Nishide, H. *Chem. Lett.* **2011**, *40*, 222.

(29) Janoschka, T.; Hager, M. D.; Schubert, U. S. *Adv. Mater.* **2012**, *24*, 6397.

(30) Wei, X.; Cosimbescu, L.; Xu, W.; Hu, J. Z.; Vijayakumar, M.; Feng, J.; Hu, M. Y.; Deng, X.; Xiao, J.; Liu, J.; Sprenkle, V.; Wang, W. *Adv. Energy Mater.* **2015**, *5*, 1400678.

(31) Brushett, F. R.; Vaughey, J. T.; Jansen, A. N. *Adv. Energy Mater.* **2012**, *2*, 1390.

(32) Zhao, Y.; Ding, Y.; Song, J.; Li, G.; Dong, G.; Goodenough, J. B.; Yu, G. *Angew. Chem., Int. Ed.* **2014**, *53*, 11036.

(33) Burkhardt, S. E.; Bois, J.; Tarascon, J.-M.; Hennig, R. G.; Abruña, H. D. *Chem. Mater.* **2013**, *25*, 132.

(34) Hernández-Burgos, K.; Burkhardt, S. E.; Rodríguez-Calero, G. G.; Hennig, R. G.; Abruña, H. D. *J. Phys. Chem. C* **2014**, *118*, 6046.

(35) Walker, W.; Grugeon, S.; Vezin, H.; Laruelle, S.; Armand, M.; Wudl, F.; Tarascon, J.-M. *J. Mater. Chem.* **2011**, *21*, 1615.

(36) Armand, M.; Grugeon, S.; Vezin, H.; Laruelle, S.; Ribiere, P.; Poizot, P.; Tarascon, J. M. *Nat. Mater.* **2009**, *8*, 120.

(37) Suttil, J. A.; Kucharyson, J. F.; Escalante-Garcia, I. L.; Cabrera, P. J.; James, B. R.; Savinell, R. F.; Sanford, M. S.; Thompson, L. T. *J. Mater. Chem. A* **2015**, *3*, 7929.

(38) Cabrera, P. J.; Yang, X.; Suttil, J. A.; Hawthorne, K. L.; Brooner, R. E. M.; Sanford, M. S.; Thompson, L. T. *J. Phys. Chem. C* **2015**, *119*, 15882.

(39) Webster, R. D.; Bond, A. M.; Schmidt, T. *J. Chem. Soc., Perkin Trans. 2* **1995**, 1365.

(40) Webster, R. D.; Bond, A. M. *J. Org. Chem.* **1997**, *62*, 1779.

(41) Carino, E. V.; Diesendruck, C. E.; Moore, J. S.; Curtiss, L. A.; Assary, R. S.; Brushett, F. R. *RSC Adv.* **2015**, *5*, 18822.

(42) Miyazaki, H.; Matsuhisa, Y.; Kubota, T. *Bull. Chem. Soc. Jpn.* **1981**, *54*, 3850.

(43) Acree, W. E.; Pilcher, G.; Ribeiro da Silva, M. D. M. C. *J. Phys. Chem. Ref. Data* **2005**, *34*, 553.

(44) Kosower, E. M.; Cotter, J. L. *J. Am. Chem. Soc.* **1964**, *86*, 5524.

(45) Kosower, E. M.; Poziomek, E. J. *J. Am. Chem. Soc.* **1964**, *86*, 5515.

(46) Leventis, N.; Rawaswdeh, A.-M. M.; Zhang, G.; Elder, I. A.; Sotiriou-Leventis, C. *J. Org. Chem.* **2002**, *67*, 7501.

(47) Solubility measurements by UV−vis indicate that saturated solutions of **9a** in MeCN have concentrations of 2.5 ± 0.1 M, which corresponds to 1.5 kg of a one-electron anolyte material per 1 kg of solvent.

(48) Williams, D. B. G.; Lawton, M. *J. Org. Chem.* **2010**, *75*, 8351.

(49) Zhang, X. M.; Bordwell, F. G.; Van Der Puy, M.; Fried, H. E. *J. Org. Chem.* **1993**, *58*, 3060.

(50) This high reactivity of **Na-9a**$^{(-)}$ is also consistent with the irreversible CVs in PC.

(51) Bordwell, F. G. *Acc. Chem. Res.* **1988**, *21*, 456.

(52) Schwarz, W. M.; Kosower, E. M.; Shain, I. *J. Am. Chem. Soc.* **1961**, *83*, 3164.

(53) Kosower, E. M.; Schwager, I. *J. Am. Chem. Soc.* **1964**, *86*, 5528.

(54) Kosower, E. M.; Poziomek, E. J. *J. Am. Chem. Soc.* **1963**, *85*, 2035.

(55) Bunce, N. J. *J. Chem. Educ.* **1987**, *64*, 907.

(56) Rate constants of 6.0×10^{-3} and 4.7×10^{-3} cm/s were measured for the reductions of **10a** to **10a**$^{(\bullet)}$ and **10a**$^{(\bullet)}$ to **10a**$^{(-)}$ at the electrode, respectively.

(57) Rheometric measurements on 0.5 and 1.0 M solutions of **10a** in MeCN reveal viscosities of 0.42 and 0.72 cP, respectively.

(58) Cabrera, P. J.; Yang, X.; Suttil, J. A.; Hawthorne, K. L.; Brooner, R. E. M.; Sanford, M. S.; Thompson, L. T. *J. Phys. Chem. C* **2015**, *119*, 15882.

(59) Huang, J.; Su, L.; Kowalski, J. A.; Barton, J. L.; Ferrandon, M.; Burrell, A. K.; Brushett, F. R.; Zhang, L. *J. Mater. Chem. A* **2015**, *3*, 14971.

(60) For example, our preliminary studies show that changing the methyl ketone to a phenyl ketone leads to a >25-fold increase in the solubility of the doubly reduced anolyte.